Science Signaling
AAAS

www.sciencesignaling.org/cgi/content/full/7/333/ra66/DC1

Supplementary Materials for

AKAP150-dependent cooperative TRPV4 channel gating is central to endothelium-dependent vasodilation and is disrupted in hypertension

Swapnil K. Sonkusare, Thomas Dalsgaard, Adrian D. Bonev, David C. Hill-Eubanks, Michael I. Kotlikoff, John D. Scott, Luis F. Santana, Mark T. Nelson*

*Corresponding author. E-mail: mark.nelson@uvm.edu

Published 8 July 2014, *Sci. Signal.* **7**, ra66 (2014)
DOI: 10.1126/scisignal.2005052

This PDF file includes:

Legends for movies S1 and S2

Other Supplementary Material for this manuscript includes the following:
(available at www.sciencesignaling.org/cgi/content/full/7/333/ra66/DC1)

Movie S1 (.wmv format). Z-stack of AKAP150 staining images across the *z* axis from the luminal surface to the SMC layer in NT mice.
Movie S2 (.wmv format). Z-stack of AKAP150 staining images across the *z* axis from the luminal surface to the SMC layer in hypertensive mice.

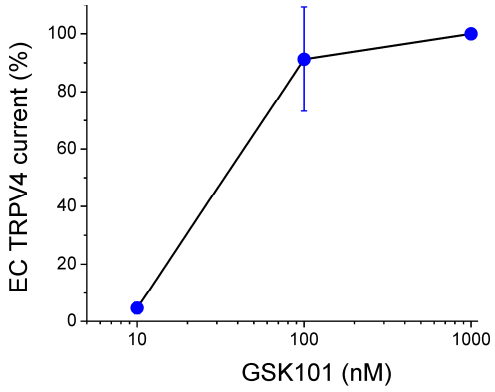

Fig. S1. Relationship between GSK101 concentration and TRPV4-mediated whole-cell K^+ currents. Currents were measured at +100 mV using the perforated-patch, whole-cell configuration in freshly isolated ECs from mesenteric arteries in the presence of 1 μM ruthenium red to prevent IK and SK channel activation and Ca^{2+} overload. The outward currents at a depolarizing potential of +100 mV were used for plotting the GSK101 concentration-response curve. The TRPV4 current density at +100 mV was 54.3 ± 5.4 pA/pF with 100 nM GSK101. Data are means ± SEM (n = 5 ECs).

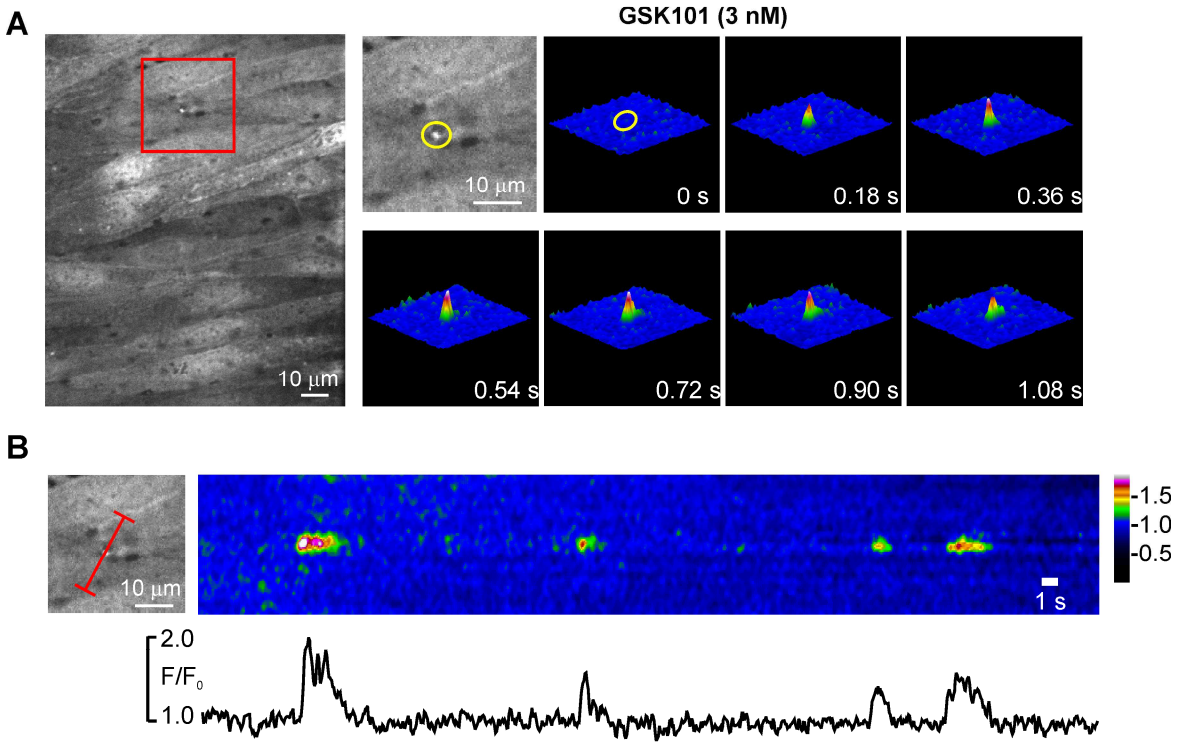

Fig. S2. TRPV4 Ca^{2+} sparklets at MEPs recorded in the presence of GSK101 and CPA. En face preparations of mesenteric arteries isolated from GCaMP2 mice were placed in a recording solution containing CPA (30 μM) and GSK101. **(A)** *Left*: Grayscale image of the endothelial surface; black holes in the autofluorescence of the internal elastic lamina indicate sites where MEPs are located. *Right*: Expanded view of the highlighted region in the grayscale image (red square) showing a three-dimensional view of the time course of a TRPV4 sparklet at a MEP site (yellow circle in small grayscale image). **(B)** A single MEP exhibits repeated sparklets. The off-line scan shows the Ca^{2+} signals in the same MEP shown in the red square in *A*. The red line indicates the region scanned.

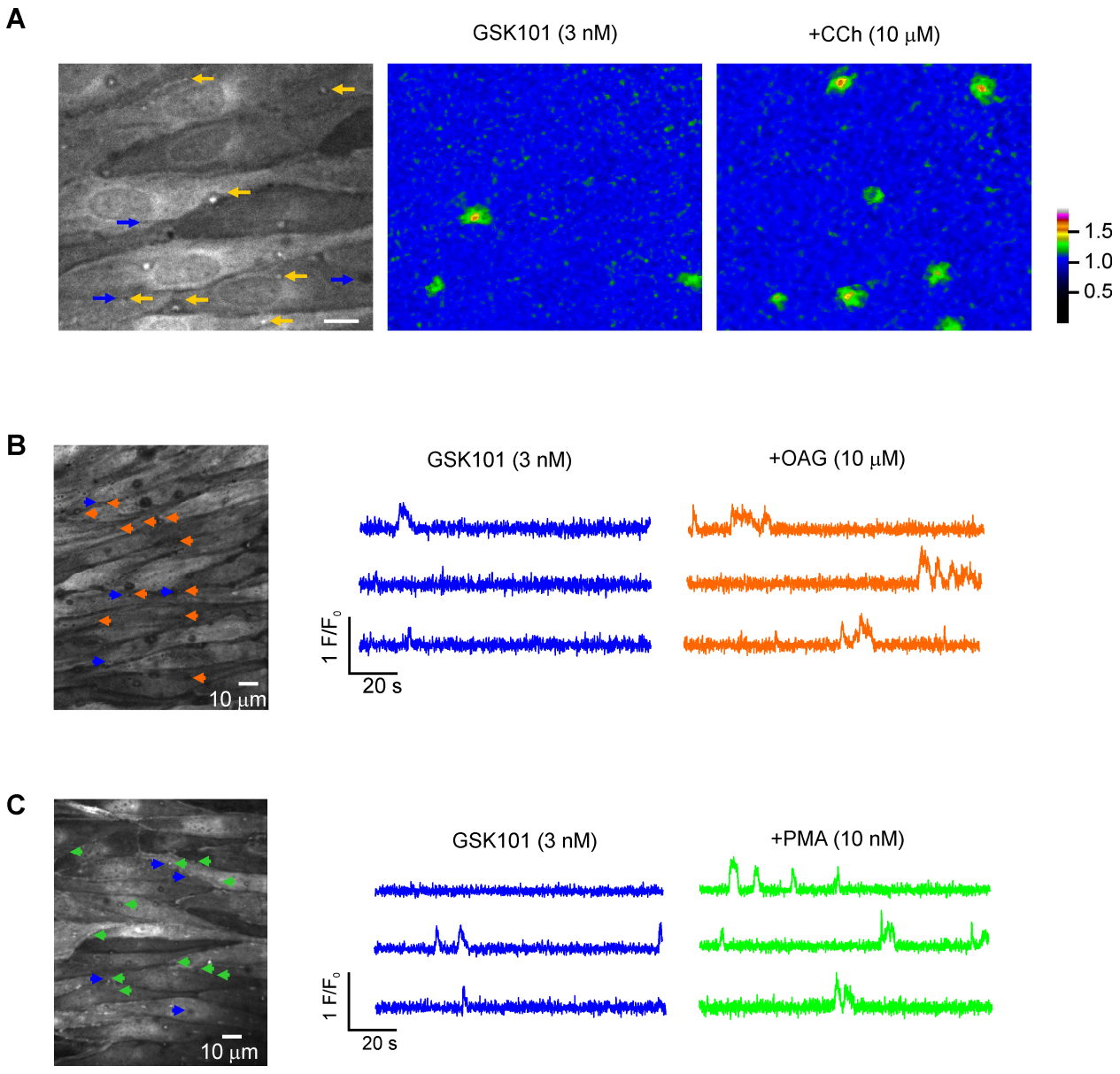

Fig. S3. CCh activates TRPV4 sparklets at MEPs through the PLC-DAG-PKC pathway in the presence of CPA and GSK101. En face preparations of mesenteric arteries isolated from GCaMP2 mice were placed in a recording solution containing CPA (30 μM) and GSK101. **(A)** Grayscale image (left) showing ~7 ECs in a field of view. Blue arrows indicate sites with MEP sparklets that were detected before the addition of CCh, and yellow arrows indicate sites with MEP sparklets that were detected after the addition of CCh. Ca^{2+} signal images show MEP sparklet sites detected before (center) and after (right) CCh addition. Each image shows the integrated activity over 2 minutes. The representative traces from this image appear in Fig. 1D. Scale bar: 10 μm. **(B)** Grayscale image (left) showing MEP sparklet sites detected before (blue) and after (orange) the addition of OAG. Representative F/F_0 traces (right) before and after the addition of OAG. **(C)** Grayscale image (left) showing MEP sparklet sites detected before (blue) and after (green) the addition of PMA. Representative F/F_0 traces (right) before and after the addition of PMA. Summary data are presented in Figure 1E.

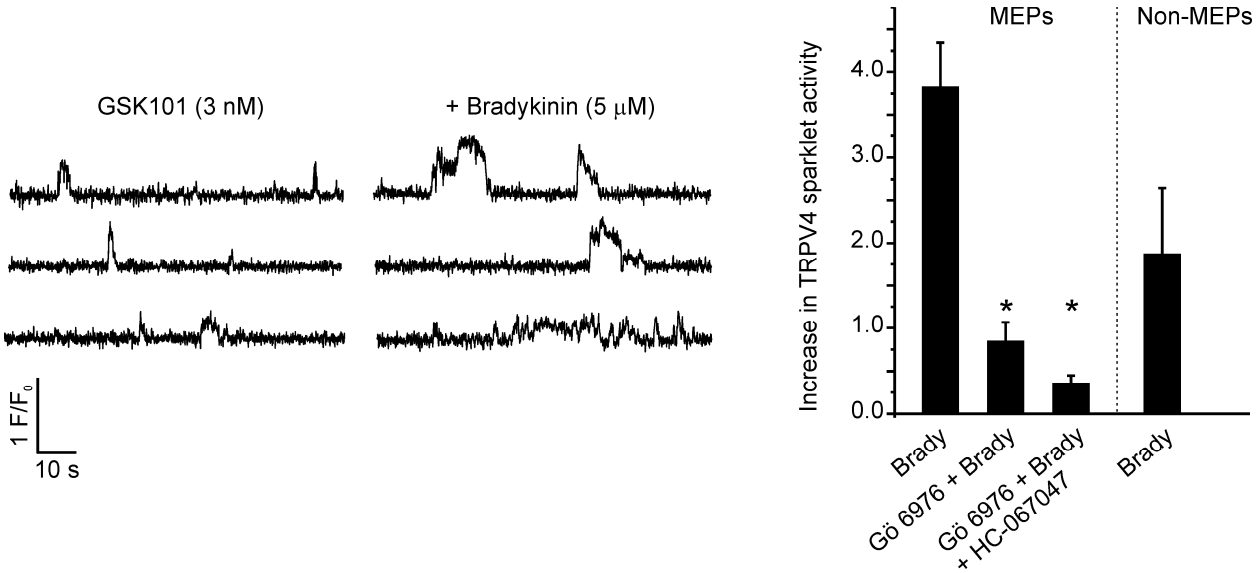

Fig. S4. Bradykinin activates TRPV4 sparklets at MEPs in a PKC-dependent manner. En face preparations of mesenteric arteries isolated from GCaMP2 mice were placed in a recording solution containing CPA (30 μM) and GSK101. *Left*, Representative F/F_0 traces from three different MEP sites before and after the addition of bradykinin (Brady). *Right*, Bar graph summarizing the effects of bradykinin on TRPV4 sparklets at MEP and non-MEP sites in the presence of GSK101 and in the presence or absence of Gö-6976 or HC-067047. Data are means ± SEM (n = 3–5). **P* < 0.05; one-way ANOVA with post hoc Bonferroni test.

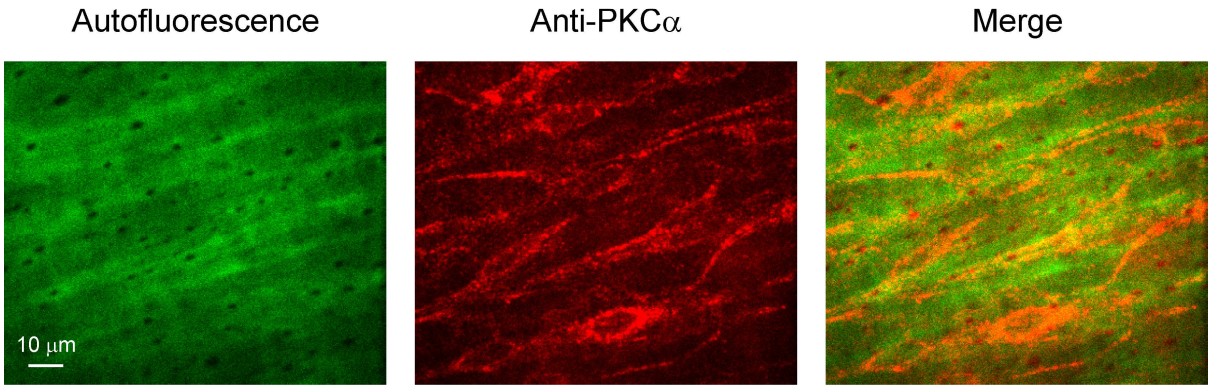

Fig. S5. PKCα is not preferentially localized at MEPs. Images of an en face preparation of a third-order mesenteric artery showing inner elastic lamina autofluorescence (*left*, green) and PKCα immunostaining in ECs (*center*, red). The merged image (*right*) shows the broad distribution of PKCα in ECs.

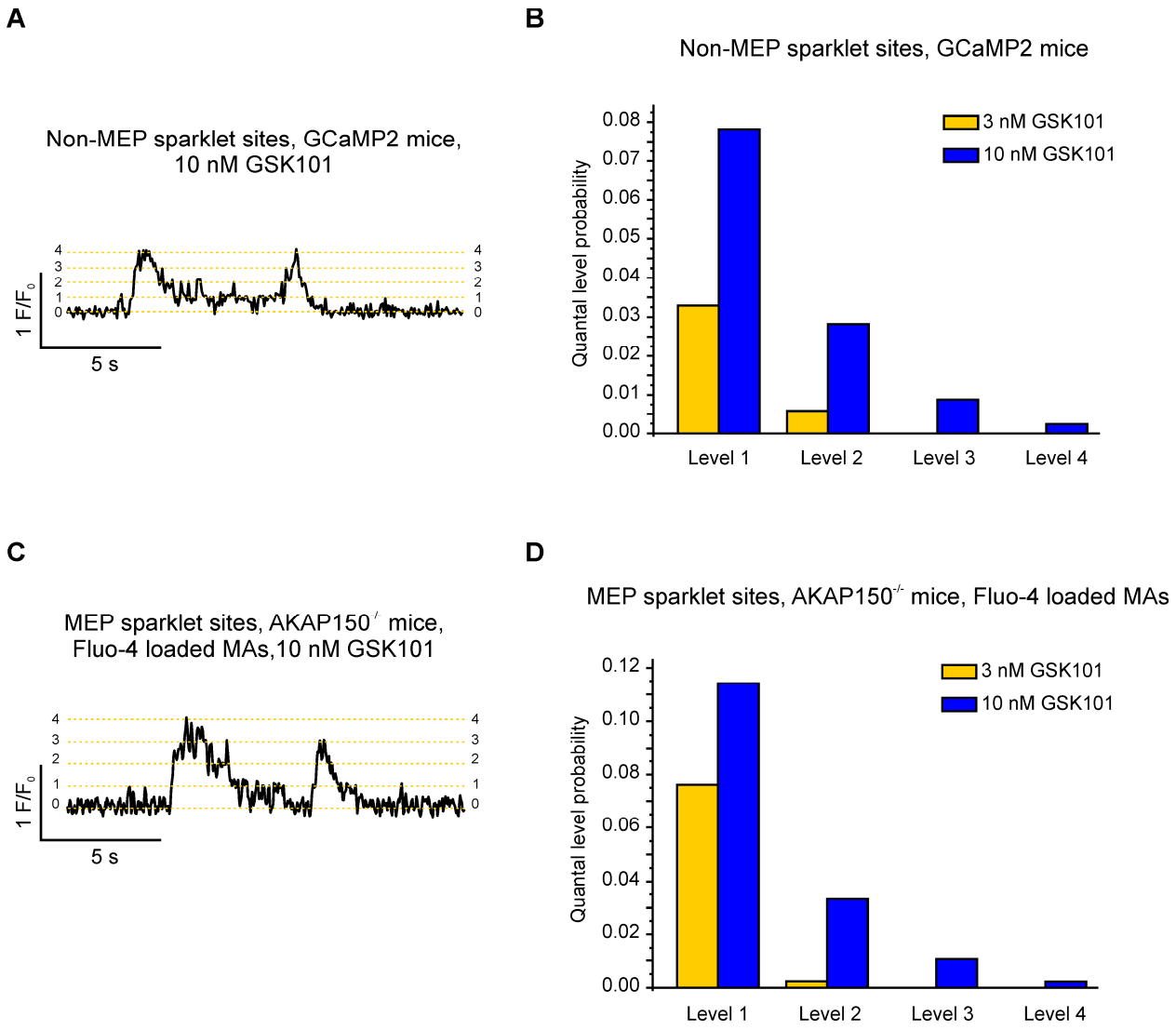

Fig. S6. Sparklet sites have a maximum of four TRPV4 channels. Quantal level response and comparisons of quantal level probability of TRPV4 sparklets at 3 nM (mustard) and 10 nM (blue) . GSK101 at non-MEP sites in control and wild-type arteries measured with GCaMP2 **(A, B)** and at MEP sites in arteries from AKAP150$^{-/-}$ mice measured with Fluo-4 **(C, D)**. Data from 6–10 fields were pooled. The total 'open duration' for mesenteric arteries from GCaMP2 mice was 2069 seconds (10 fields from 9 arteries). The corresponding value for mesenteric arteries from AKAP150$^{-/-}$ mice was 1228 seconds (6 fields, 3 arteries).

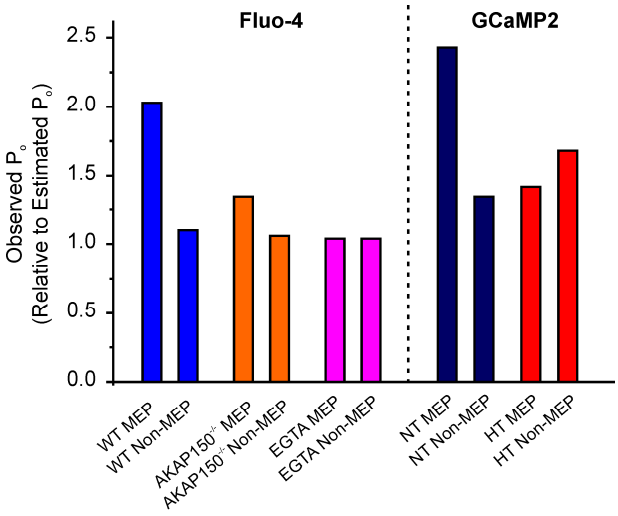

Fig. S7. Ratio of the experimentally observed P_O of TRPV4 channels to the P_O predicted by the binomial distribution assuming independent gating of TRPV4 channels. Intracellular Ca^{2+} was measured with Fluo-4 (left side) and GCaMP2 (right side) at a frame rate of 30/s and 15/s, respectively. A ratio of 1 would be indicative of independent gating. Data from 7-10 arteries were pooled.

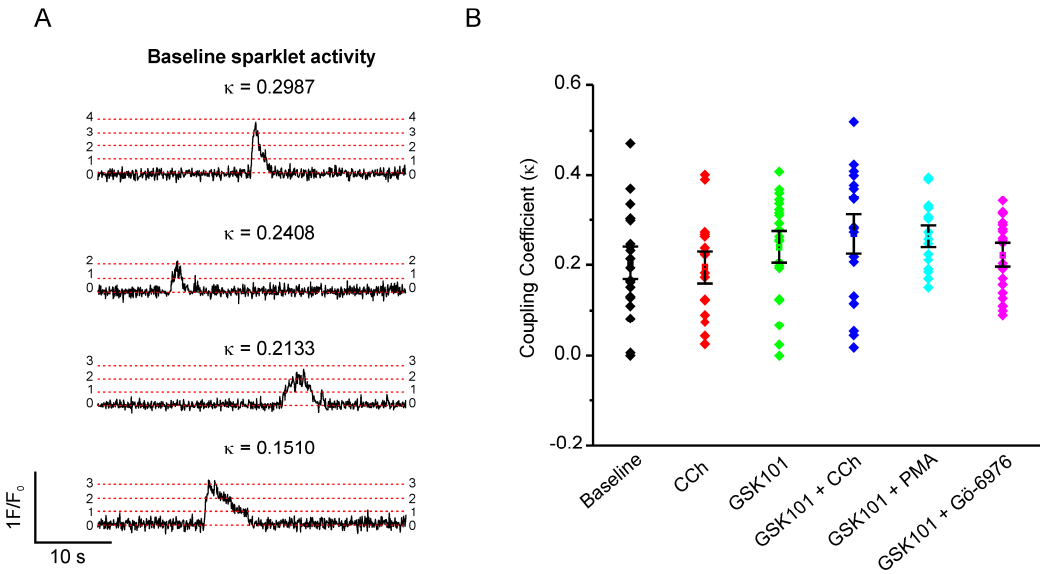

Fig. S8. Inhibition or activation of the GqPCR-PKC-TRPV4 pathway does not alter the functional coupling of TRPV4 channels. Coupling coefficients (κ) were calculated in the presence of CCh (10 μM), the PKC activator PMA (10 nM), the PKC inhibitor Gö-6976 (1 μM), and/or the TRPV4 channel agonist GSK101 (3 nM), as indicated. **(A)** Representative F/F_0 traces with respective κ-values for baseline TRPV4 sparklet activity at MEP sites (no GSK101). **(B)** A scatter plot of individual κ-values along with means ± SEM (black error bars) for each group (n = 16–22 sites).

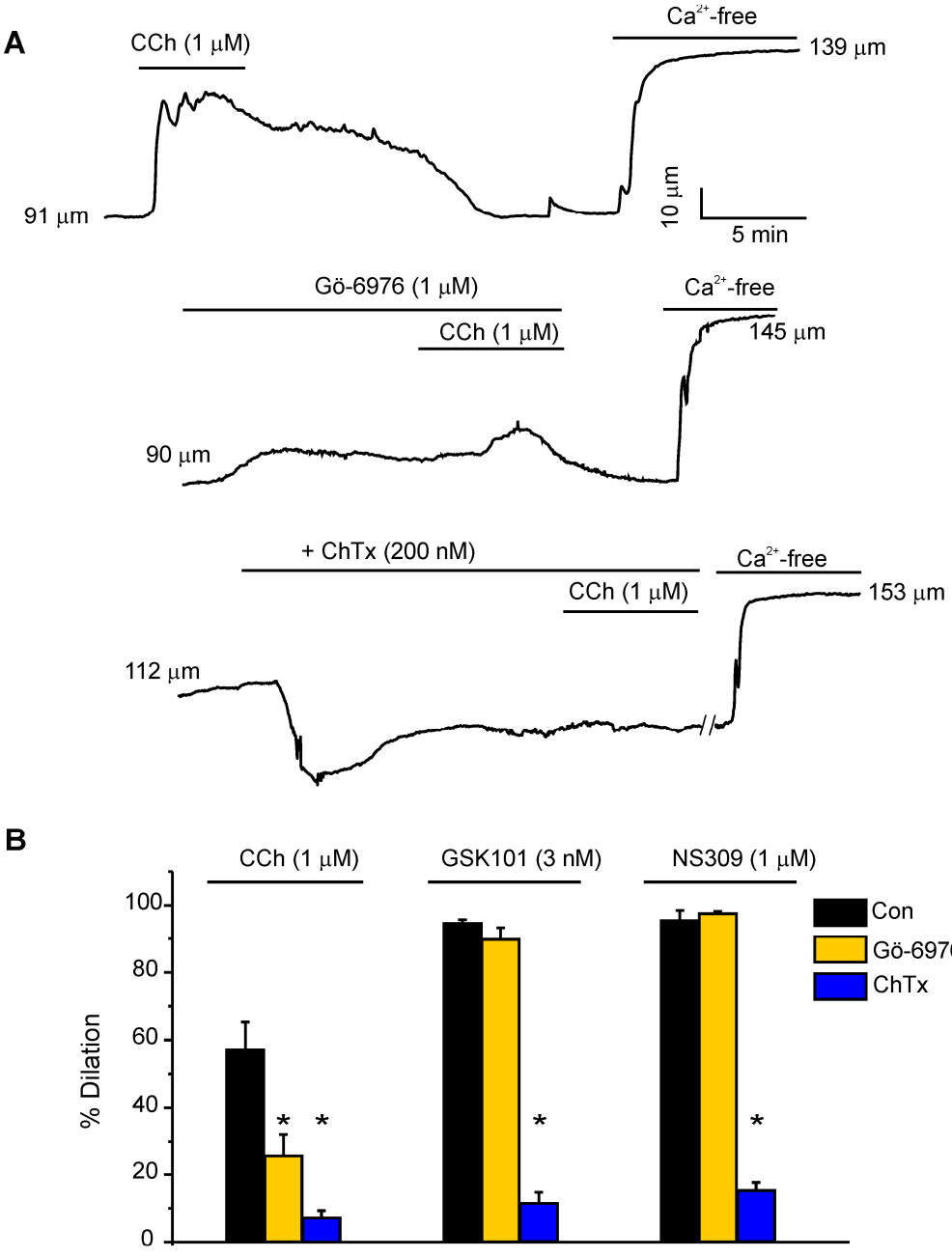

Fig. S9. Inhibition of PKC or IK channels attenuates dilation to CCh. Measurements were made in pressurized (80 mm Hg) mesenteric arteries in the presence of L-NNA (100 μM) and indomethacin (10 μM). **(A)** Diameter traces illustrating dilations to CCh in the absence (upper trace) and presence (middle trace) of the PKC inhibitor Gö-6976 or IK channel blocker charybdotoxin (ChTx, lower trace). **(B)** Bar graph showing the effect of Gö-6976 or ChTx on dilation to CCh, GSK101, or NS309 (IK and SK activator) (n = 4–6 arteries). Control (Con) for each bar set corresponds to treatment with (left to right) CCh, GSK101, or NS309 alone. Maximum dilation is defined as $Diameter_{Ca^{2+}\text{-free}} - Diameter_{basal}$. Basal diameter was defined as the diameter in the presence of myogenic tone, before addition of a drug. *P < 0.05, one-way ANOVA with post hoc Bonferroni test.

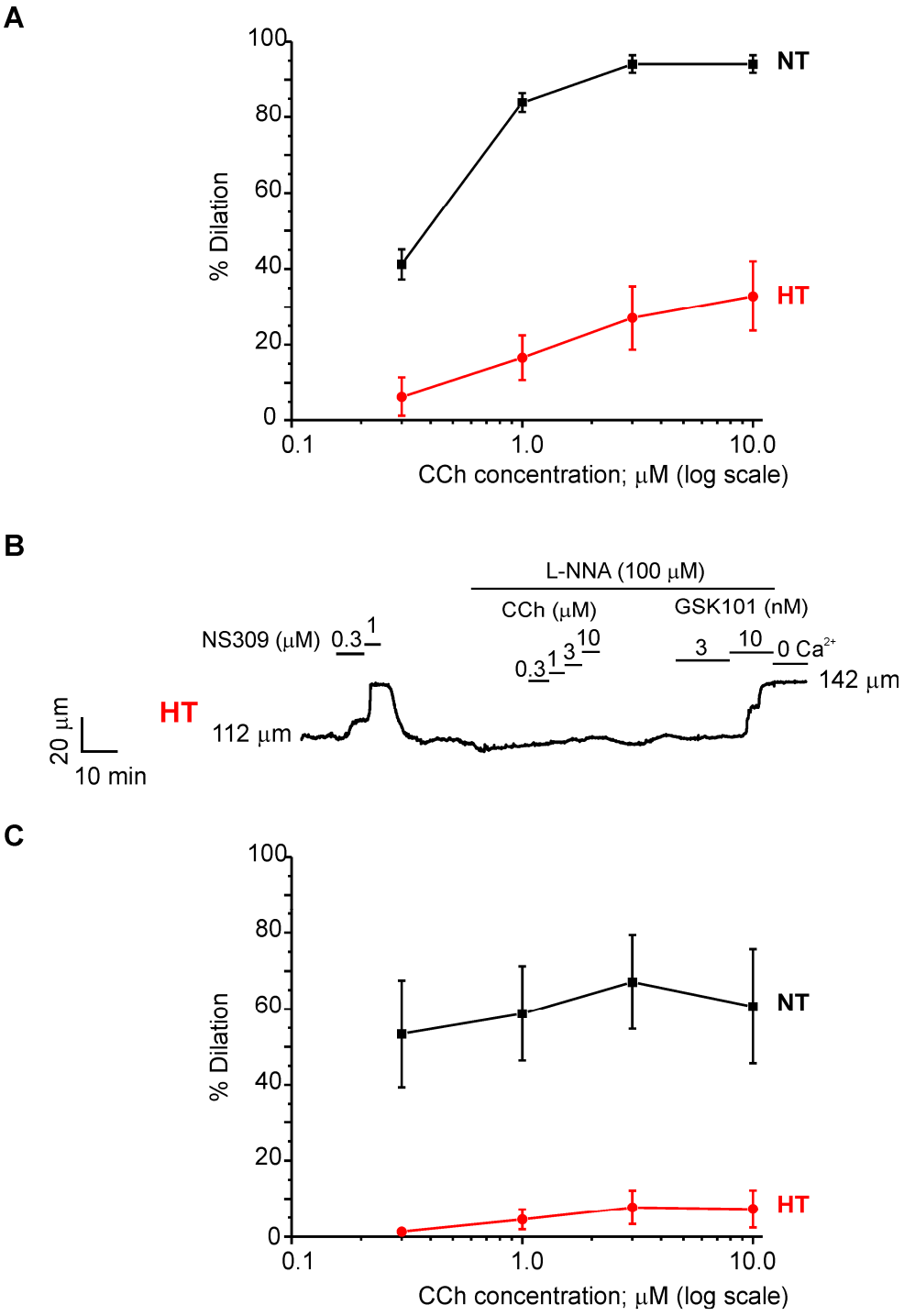

Fig. S10. The EDH component of CCh-induced vasodilation is abolished in Ang II–induced hypertension. (A) The relationship between CCh concentration and dilation of pressurized (80 mm Hg) mesenteric arteries from normotensive (NT) and hypertensive (HT) mice. **(B)** A representative diameter trace illustrating dilations of a pressurized mesenteric artery from a HT mouse to CCh and GSK101 in the presence of L-NNA (100 μM), included to inhibit NO production. **(C)** Concentration-dilation relationship of CCh in the presence of L-NNA in pressurized mesenteric arteries from NT and HT mice (n = 5 arteries from 5 mice).

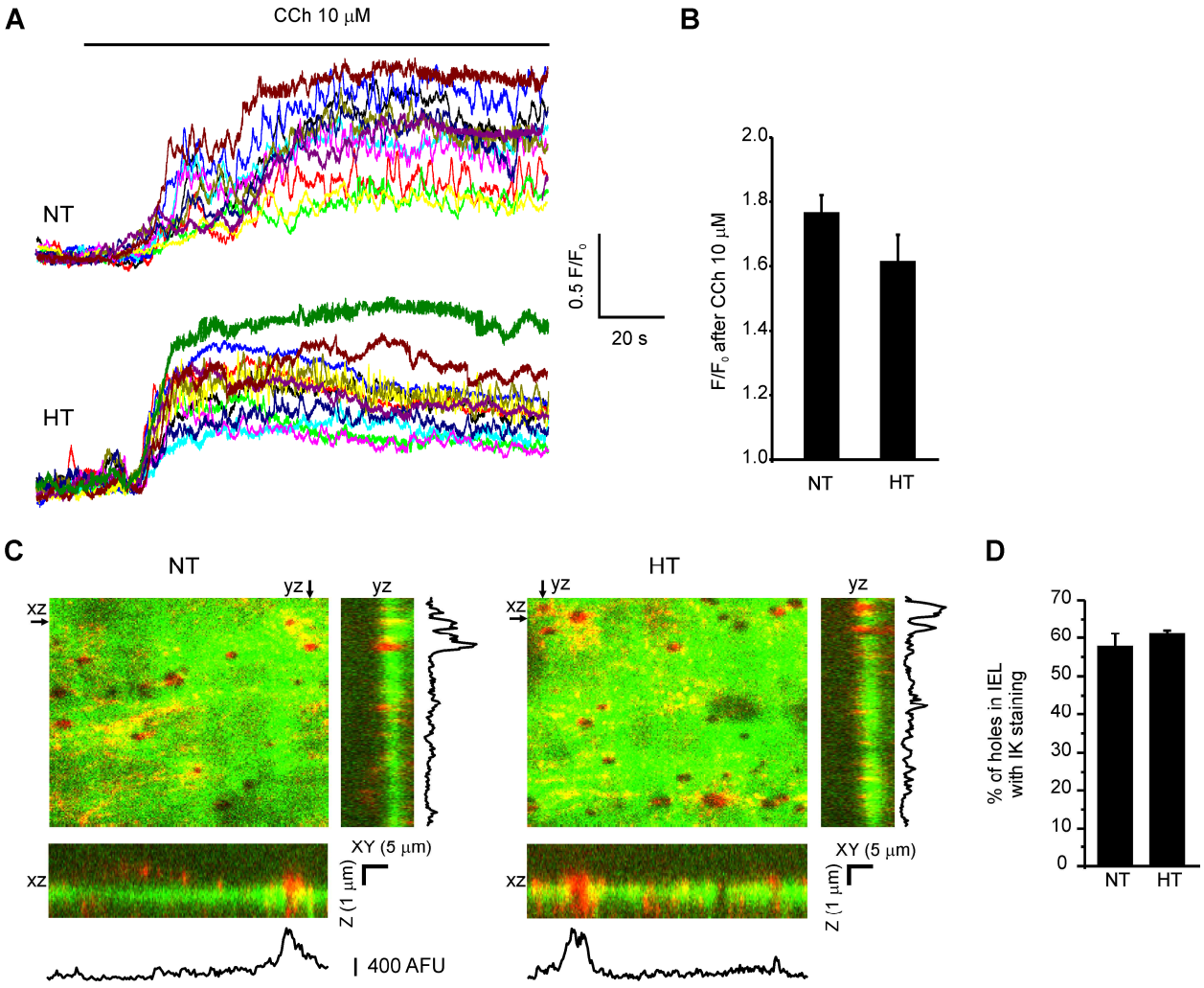

Fig. S11. CCh-induced increases in whole-cell Ca^{2+} in ECs and IK channel localization at MEPs are unaltered in hypertension. (A) Whole-cell Ca^{2+} was imaged in en face preparations from mesenteric arteries. The different color tracings correspond to recordings from individual cells (n = 41–47 cells, 4–5 arteries from 4–5 mice) using each cell outline as an ROI (not shown). **(B)** F/F_0 was averaged over 10 seconds from the time of peak fluorescence intensity following CCh addition. **(C)** Three-dimensional views along the z-axis (0.1-μm optical slices) showing densities of IK channel fluorescence projecting through the depth of the inner elastic lamina in NT and HT mice. Reconstructed xz- and yz-images of IK channel immunostaining along the MEP, showing strongest staining towards the end of the projections. Traces are plot profiles for IK channel staining along x- and y-axes for 5-μm-wide transects through the projections shown in the three-dimensional views. **(D)** Bar graph indicates the number of holes in the inner elastic lamina with IK channel staining, defined as peak staining within 5 μm of the center of a hole (n = 4–5).

Table S1. Number and density of IK, SK, and TRPV4 channels in ECs.

	Channels per EC	Channel density (per 10 μm^2)
TRPV4	170	1.2
IK	757	5.2
SK	339	2.3

Table S2. Internal diameters of CCh-dilated third-order mesenteric arteries from NT and hypertensive mice.

	NT	HT
ID, baseline at 80 mm Hg	95.2 ± 5.6 (6)	106.7 ± 7.8 (5)
CCh, 0.3 μM	112.5 ± 4.7 (6)	106.6 ± 12.8 (5)
CCh, 1.0 μM	131.5 ± 5.4 (6)	111.2 ± 14.3 (5)
CCh, 3.0 μM	136.4 ± 8.3 (5)	115.6 ± 14.4 (5)
CCh, 10.0 μM	136.4 ± 8.3 (5)	118.0 ± 14.5 (5)
Ca^{2+}-free diameter at 80 mm Hg	138.3 ± 6.2 (6)	147.6 ± 14.1 (5)

Numbers in parentheses indicate n-values. Data are presented as the average ± SEM.
ID, internal diameter (μm); NT, normotensive; HT, hypertensive.

Table S3. Internal diameters of GSK101-dilated third-order mesenteric arteries from NT and hypertensive (HT) mice.

	NT	HT
ID, baseline at 80 mm Hg	103.6 ± 6.2 (7)	98.4 ± 13.4 (5)
GSK101, 3 nM	146.7 ± 6.0 (7)	109.0 ± 14.9 (5)
Ca^{2+}-free diameter at 80 mm Hg	146.0 ± 5.7 (7)	139.8 ± 14.3 (5)

Numbers in parentheses indicate n-values. Data are presented as the average ± SEM.
ID, internal diameter (μm); NT, normotensive; HT, hypertensive.

Table S4. General properties of mesenteric arteries and ECs from NT and hypertensive (HT) mice.

	NT	HT
ID, baseline at 80 mm Hg (μm)	107.3 ± 3.6 (13)	106.8 ± 5.8 (13)
Ca^{2+}-free diameter at 80 mm Hg (μm)	148.3 ± 4.3 (13)	148.2 ± 5.9 (13)
Myogenic tone at 80 mm Hg (% of Ca^{2+}-free diameter)	27.6 ± 1.2 (13)	28.4 ± 1.5 (13)
Holes in the IEL/EC	4.6 ± 0.2 (6)	4.7 ± 0.2 (6)
Holes/field	66.8 ± 3.5 (5)	67.7 ± 2.9 (5)
Average diameter of holes in the IEL (μm)	2.3 ± 0.1 (4)	2.4 ± 0.1 (4)
Wall thickness (μm)	15.1 ± 0.9 (6)	23.9 ± 1.0 (7)
ECs/field of view	14.4 ± 0.5 (11)	14.5 ± 0.3 (11)
IEL depth (μm)	1.6 ± 0.04 (6)	1.6 ± 0.03 (6)
ID, 0.3 μM NS309 (μm)	116.7 ± 2.7 (12)	113.6 ± 7.0 (12)
ID, 0.6 μM NS309 (μm)	134.6 ± 6.7 (8)	128.5 ± 7.7 (5)
ID, 1.0 μM NS309 (μm)	149.3 ± 4.2 (12)	145.9 ± 6.1 (13)
EC capacitance (pF)	14.6 ± 0.7 (11)	14.0 ± 1.8 (13)

Data are presented as the average ± SEM. Numbers in parentheses indicate n-values.
ID, internal diameter; IEL, internal elastic lamina; NT, normotensive; HT, hypertensive.

Movie S1. Z-stack of AKAP150 staining images across the *z* axis from the luminal surface to the SMC layer in NT mice. Scale bar: 10 μm.

Movie S2. Z-stack of AKAP150 staining images across the *z* axis from the luminal surface to the SMC layer in hypertensive mice. Scale bar: 10 μm.